SSIM 2025 - JJ Potter & J Wesseloo (eds)

doi:10.36487/ACG_repo/2535_21

Long-term instability of the East Archimedes slope failure headscarp: a case history

Blake Easby [a,*], Jared Mullenbach [a], Rachel Becker [a], Timothy George [b]

[a] *WSP, USA*

[b] *i-80 Gold Corp., USA*

Abstract

In late 2013, the south highwall of the East Archimedes open pit at the Ruby Hill mine collapsed after many months of detailed monitoring and analysis, leaving behind a near-vertical 90 m high headscarp. The south highwall consists of cemented alluvium that performed very well in previous phases of mining at slope angles steeper than 55°. The mechanism of failure was postulated to be due to deformation of the underlying intrusive rock in response to stress relaxation of the rock mass during mining, and shear strain localisation at the base of the alluvium resulting in a weakening of the materials at or near the contact between the alluvium and underlying rock.

Since the initial slope failure, the headscarp remained near-vertical with relatively little additional deformation, with the exception of some surficial spalling and ravelling from the headscarp face. In 2021, additional mining was completed in the bottom of the pit, opposite the slope failure and headscarp. In the winter of 2022, nearly 9 years after the 2013 failure and approximately 3 months after mining in the bottom of the pit was completed, a substantial portion of the headscarp failed. Following, additional smaller failures of the headscarp in the same region occurred. This paper aims to review the mechanism of failure in the 2013 and 2022 events to better understand the relationship between mining in the pit and the stability of the headscarp.

Keywords: *cemented, alluvium, instability, case history, Nevada*

1 Introduction

The Ruby Hill mine is a past-producing open pit gold and silver mining operation located in Eureka County, Nevada, within the Basin and Range province of the western United States. The Basin and Range province is a physiographic region characterised by alternating mountain chains and valleys that are the result of continental crustal extension and faulting. The region has an arid to semi-arid climate with sparse vegetation and rugged topography with significant relief between mountain ranges and adjacent basins. The local geology is complex, composed of sedimentary rocks intruded by igneous units, and overlain by cemented alluvial deposits that range in mechanical characteristics of a coarse-grained soil to a strong rock. The location of the Ruby Hill mine and the East Archimedes pit is shown in Figure 1.

[*] Corresponding author. Email address: blake.j.easby@wsp.com

Figure 1 Project location and East Archimedes pit aerial view

In October 2010, the south highwall of the East Archimedes pit began to exhibit indications of instability in the form of cracking and displacement of the benches and working levels. In November 2013, approximately 3 years after the initial indications of deformation were observed, the slope collapsed resulting in an approximately 7 million tonne failure and the formation of a near-vertical, 90 m high headscarp. Following the 2013 failure, mining operations in the East Archimedes pit were suspended, due in part to the challenges associated with remediation of the failed slope. The headscarp remained largely intact and near-vertical for nearly a decade, with only minor surficial spalling and ravelling observed.

In 2021, following an approximately 9 year hiatus to mining, limited mining resumed in the bottom of the East Archimedes pit to extract ore from approximately five benches on the north side of the pit (opposite the failure). Approximately three months after mining in the bottom of the pit had been completed, a significant portion of the headscarp, collapsed in the spring of 2022. Several subsequent, smaller failures have occurred in the same area over the following years.

2 Geologic setting

The bedrock geology of the East Archimedes pit is composed primarily of Ordovician limestones (Og) and a younger rhyolitic intrusive unit (Kgf). These are overlain by tuffs (Trt) and alluvial deposits (Qal and Tal) which range in thickness from a few metres to a few hundreds of metres. In some areas, the Tal is present and the Trt is absent, and vice versa. Where both are present, the Tal overlies the Trt. A younger cemented alluvial deposit (Qal) overlies the Trt and the Tal. The Qal ranges in thickness from about 140–180 m in the area of the 2013 slope failure, and the intrusive bedrock surface dips into the pit at about 5–20°. The Tal unit is distinct from the overlying younger alluvium in both texture and composition, consisting primarily of intrusive-derived matrix and clasts, in contrast to the limestone-dominated clasts found in the overlying younger alluvium. The Trt is composed of air fall tuffs and dacitic flows that directly overlie the bedrock under the Qal and Tal.

The regional groundwater table is approximately 180 m below ground surface in the vicinity of the pit and groundwater is generally kept below the pit bottom elevation with pumping wells and horizontal drains.

3 2013 event

The November 2013 failure was preceded by cracking that was first observed in September 2010. The cracks ranged in length from approximately 6–50 m contiguously and extended across multiple benches. Slope monitoring in 2010 included prism monitoring with a robotic total station. Other common types of remote monitoring, such as radar systems, were not used. At that time, higher displacements were observed in the Og and Kgf bedrock units below the Qal, as shown in Figure 2.

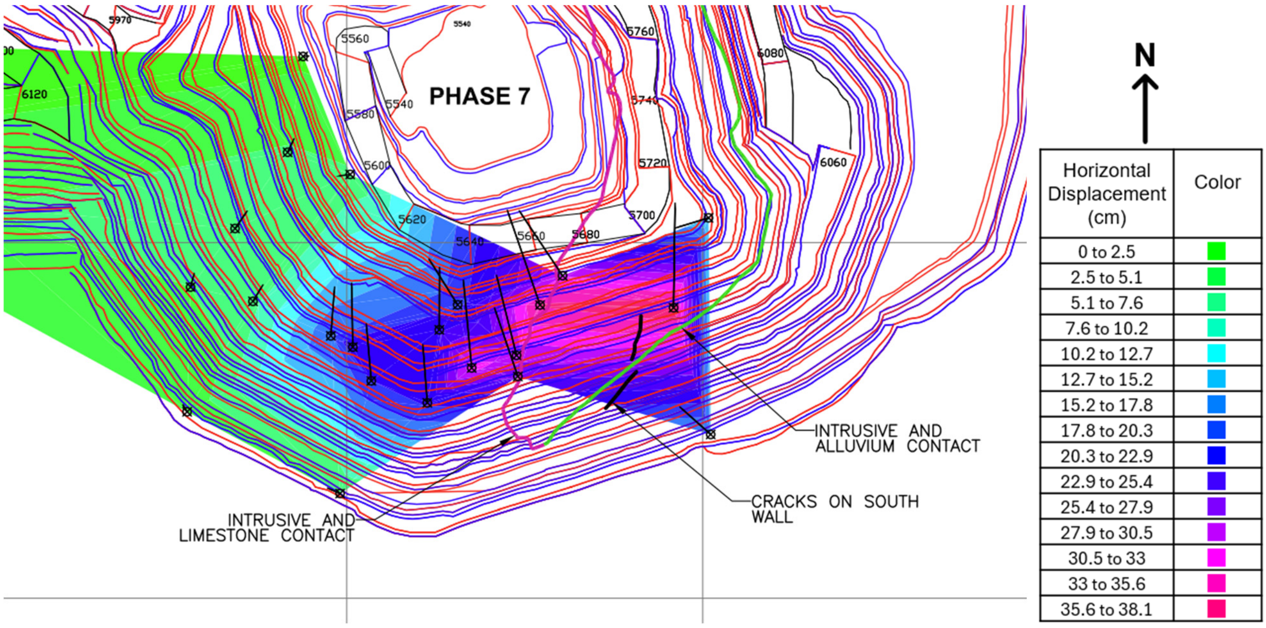

Figure 2 2010 prism displacement heat map

Displacements continued from June 2010 to July 2011 but began to slow in mid-2011. The reduction in displacement rate was attributed to additional dewatering of the slopes from pumping wells and horizontal drains in the bedrock.

In June 2013, deformation of the slope began to steadily accelerate. Mining was occurring in the southeast portion of the East Archimedes pit, in the approximate area shown in red in Figure 3, from elevations 1,774–1,737 m (5,820–5,700 ft), until October 2013. Accelerated deformation rates in October indicated the slope was progressing toward failure, and additional prisms were installed on the south slope, spanning multiple benches and the pit crest. Mining operations were relocated to another area of the pit until mine technical staff cleared the entire pit in preparation of the failure.

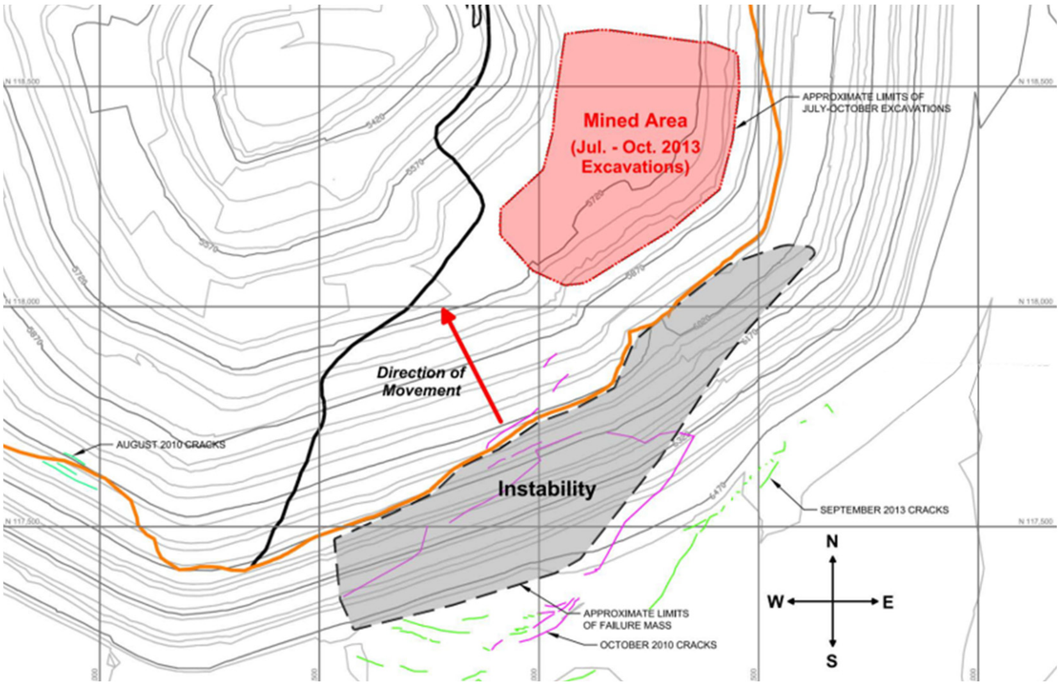

Figure 3 Southeast slope area with approximate instability bounds and surface cracking

A radar system was acquired from a separate nearby operation owned by the operator and installed in the East Archimedes pit. Unlike the 2010 displacements, where higher displacements were concentrated in the bedrock, the displacements observed in 2013 were higher within the Qal unit. A distinct change in displacement rates was clear at the base of the Qal directly above the intrusive, as shown in Figure 4. Displacements also were measured in the underlying intrusive, though at lower magnitudes.

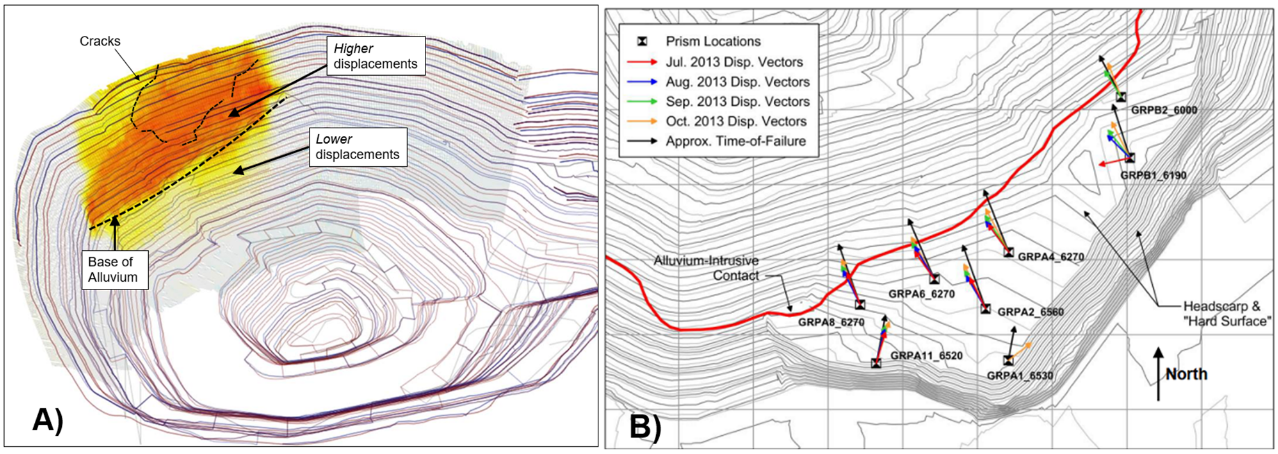

Figure 4 (a) Radar monitoring heat map; (b) Prism vectors preceding the 2013 failure

Following the slope collapse in November 2013, a geotechnical investigation was conducted to characterise the slope conditions immediately behind the failed slope to better understand the contributing factors of the failure, with a focus on the materials at the base of the Qal and above the underlying bedrock. The investigation included geotechnical drilling, core logging, and laboratory testing. Eighteen vertical and inclined coreholes were drilled behind the pit crest, and geotechnical core logging was completed at the rig to characterise the materials and collect samples. Inclinometer casing was installed in 2 of the coreholes for ongoing monitoring. Laboratory testing on samples collected during the drilling investigation included particle size distribution, Atterberg limits, and unit weight tests for the Qal, Tal, and Trt units. Rock strength testing on the Qal included unconfined compressive strength (UCS), triaxial compressive strength, and Brazilian tensile strength tests. Consolidated undrained triaxial (CIU) tests were performed on intact Tal and Trt samples.

3.1 Engineering characterisation

The Qal is variably cemented by calcium carbonate precipitation (also known as Caliche) which is common in arid and semi-arid regions. An observation-based classification system was used during early geotechnical investigations to describe the degree of cementation within the alluvium. This system includes 4 classes: uncemented, weakly cemented, moderately cemented, and strongly cemented. The classes were assessed by estimates of the relative hardness and reaction to hydrochloric acid. Estimates of the distribution of cementation based on drilling data are summarised in Table 1.

Table 1 Estimated distribution of cementation within the alluvium

Degree of cementation	Estimated percentage of alluvium
0–1	10–20
1–2	60–70
2–3	20–30

Laboratory and field testing on core samples of the alluvium indicated a wide range of UCS values ranging from approximately 1 MPa (extremely weak rock – R0) to up to 70 MPa (strong rock – R4). An example of a strongly cemented Qal core is shown in Figure 5. Testing indicated friction angles of the Qal samples to range from 43° to as high as 60°.

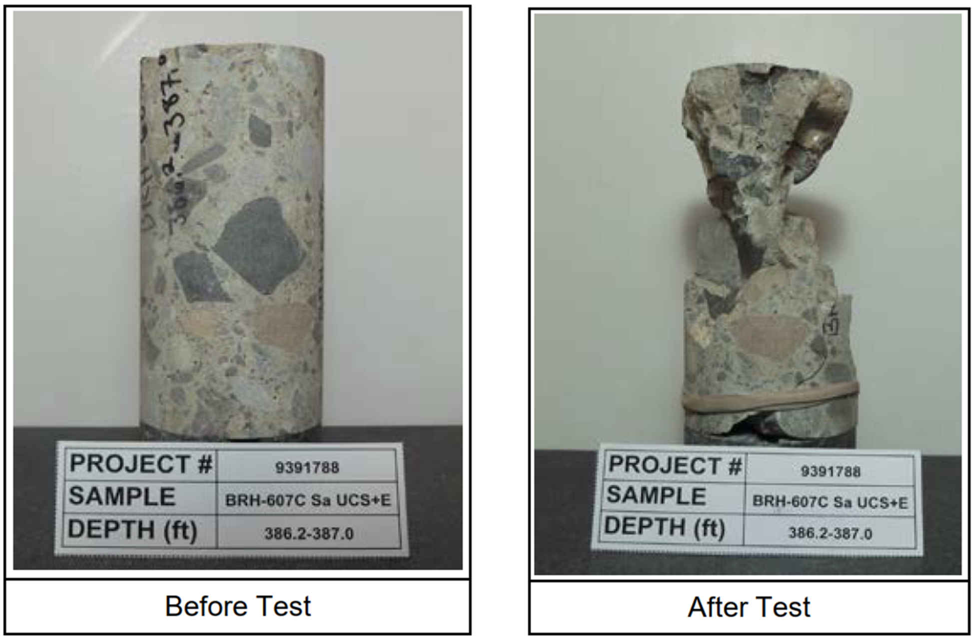

Figure 5 Strongly cemented alluvium core sample from the south wall of the East Archimedes pit

The Tal and Trt materials are soil-like and generally uncemented. In the vicinity of the failure and immediately below the Qal, the materials were similar in composition and plasticity. Grain size distribution testing on the Tal samples used for strength testing indicated fines contents ranged from 36–70% (with clay content ranging from 17–50%) and a plasticity index of between 12 and 45. The samples classified as (according to the unified soil classification system [USCS]) (ASTM International 2025) clayey sand (SC), silty sand (SM), and silty gravel (GM), sandy silt (MH), and sandy clay (CH). Grain size distribution testing on the Trt samples used for strength testing indicated fines contents ranged from 37–61% (with clay content ranging from 15–31%) and plasticity indices ranged from 13–36. The Trt is classified as clayey sand (SC), silty sand (SM), sandy silt (MH), and sandy clay (CH).

The CIU testing of many of the Tal and Trt samples indicated a significant reduction from peak shear strength to residual strength, indicating strain-weakening behaviour.

3.2 Slope stability analyses

Slope stability of the 2013 failure was evaluated using two-dimensional (2D) and three-dimensional (3D) limit equilibrium analyses, and 2D numerical (FLAC) analyses. 2D limit equilibrium analyses were completed using Rocscience Slide2 and 3D limit equilibrium analyses were completed using SVSlope3D. Figure 6 shows the conceptual model used in the slope stability analyses and an example output of the 3D limit equilibrium stability analysis is shown in Figure 7.

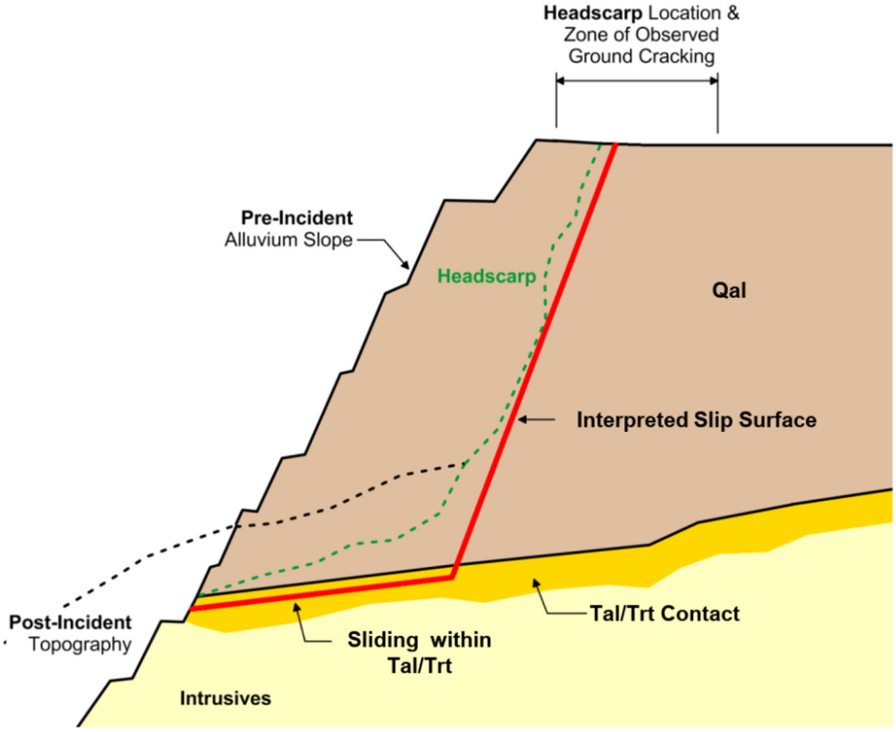

Figure 6 Generalised cross-section and conceptual model of the of the southeast wall

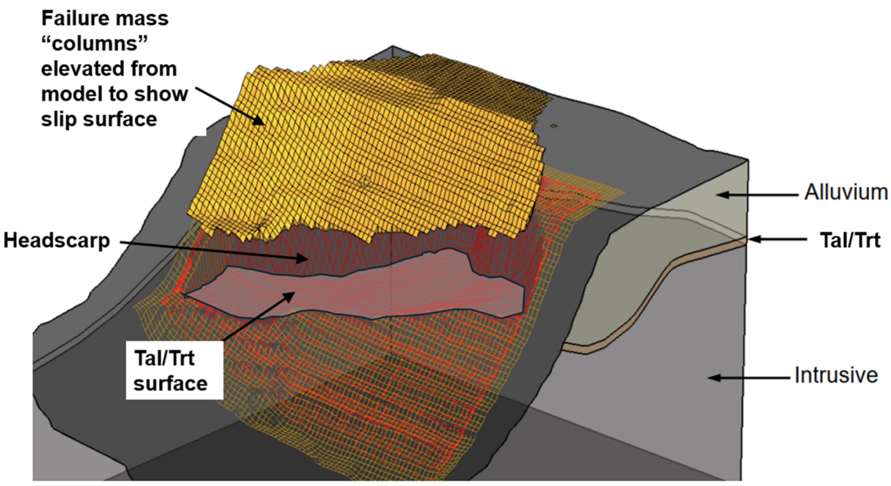

Figure 7 Example 3D limit equilibrium slope stability analysis output

Shear strength parameters for the Qal and Tal/Trt units were developed from laboratory testing and calibrated using the models. For the Qal, a nominal friction angle of approximately 45°, representing a best-fit through the range of the test data, was used as a starting point for calibration. The back-calculated cohesion values ranged from 21–27 psi based on the back-analyses.

Because the distribution of the Tal and Trt was not well defined, a single material was modelled at the base of the Qal to represent both the Tal and Trt. Back-calculated friction angles for this unit ranged from 16–22° with no cohesion, which was consistent with the laboratory-derived residual shear strengths. As the identified critical slip surface was above the watertable, groundwater pressures were not included. A summary of the material properties developed from laboratory testing and back-analyses is provided in Table 2.

Table 2 Summary of material properties based on laboratory testing and back-analyses

Geologic unit	Unit weight (kN/m³)	Strength model	Friction angle (degrees)	Cohesion (kPa)
Alluvium (Qal)	25	Peak	45[1]	145–1,862
Contact material (Tal and Trt)	20	Peak	21–25[1]	310–331[1]
	20	Residual	16–22[2]	0[2]

Notes:
[1] Interpreted from laboratory testing.
[2] Interpreted from back-analyses and laboratory testing.

4 2022 event

In August 2020, a relatively small mine plan consisting of approximately 5 benches on the north side of the East Archimedes pit (red shaded area in Figure 8) was initiated to recover additional ore in the bottom pit.

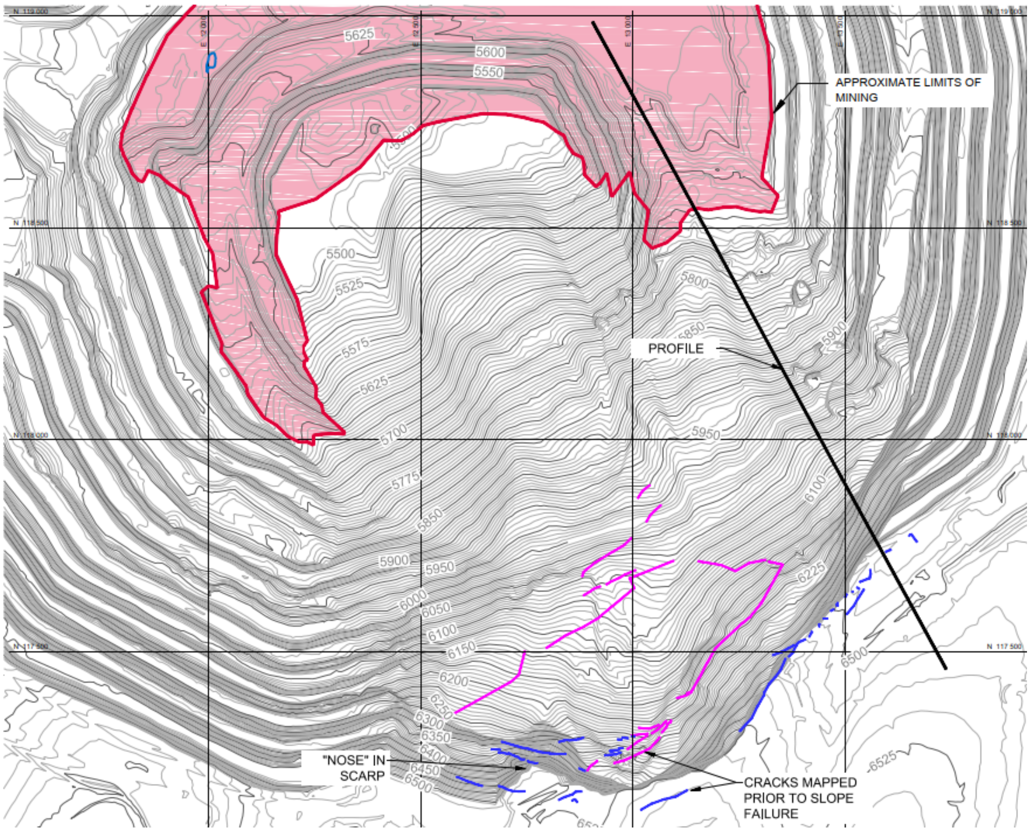

Figure 8 Portion of north side of East Archimedes pit mined in 2021

Mining occurred over an approximately 16 month period from August 2020 to November 2021. Upon completion of mining, access to the bottom of the pit was blocked, and radar monitoring was discontinued. In the winter of 2022, a substantial portion of the 2013 failure headscarp collapsed, depositing failure debris into the recently mined area. Additional smaller failures of the headscarp continued to occur in the same area through July 2024 (Figure 9). Unfortunately, details and monitoring of the 2022 failure are limited as there was a lapse in monitoring of the prism monuments located on the crest of the headscarp due to an equipment malfunction. Regular monitoring of the 2 existing inclinometers did not show signs of large-scale instability leading up to the failure. As there were no mining activities in the East Archimedes pit at the time, there were no observations of the failure until after it occurred.

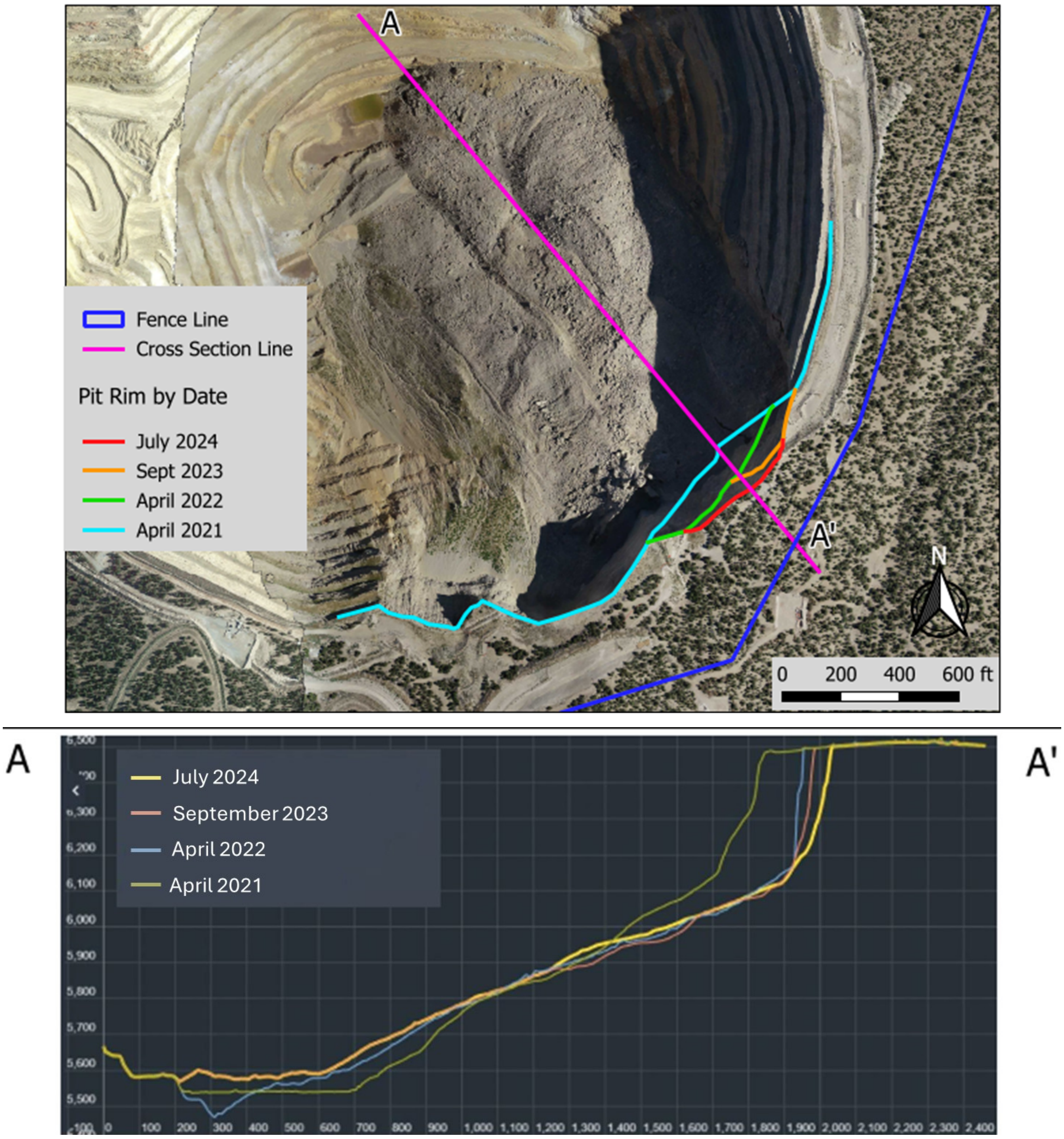

Figure 9 Section A-A′ showing slope profiles from 2021, 2022, 2023, and 2024

A 2D FLAC numerical analysis with a strain-weakening material model for the Tal/Trt was also performed shortly after the 2013 event when evaluating various mitigation strategies following the 2013 event. Interestingly, the failure mechanism closely resembles the failure that had not yet occurred in 2022, supporting the model as a useful predictor of future performance. The strain-weakening model employed included a gradual reduction in friction angle and cohesion based on the strain level and was based on the results of the laboratory testing. The mass stiffness (Young's modulus) of the Qal was approximately 2 times the Young's modulus of the Tal/Trt and the model was run in stages to simulate the stress redistribution result of future mining.

Figure 10 presents the results of the 2D FLAC analysis, showing strain localisation in the Tal/Trt. The benching shown is a conceptual mine plan that would reduce the slope angle of the headscarp. The section analysed corresponds approximately to cross-section A-A' (refer to Figure 9), which is within the portion of the slope that collapsed in 2022.

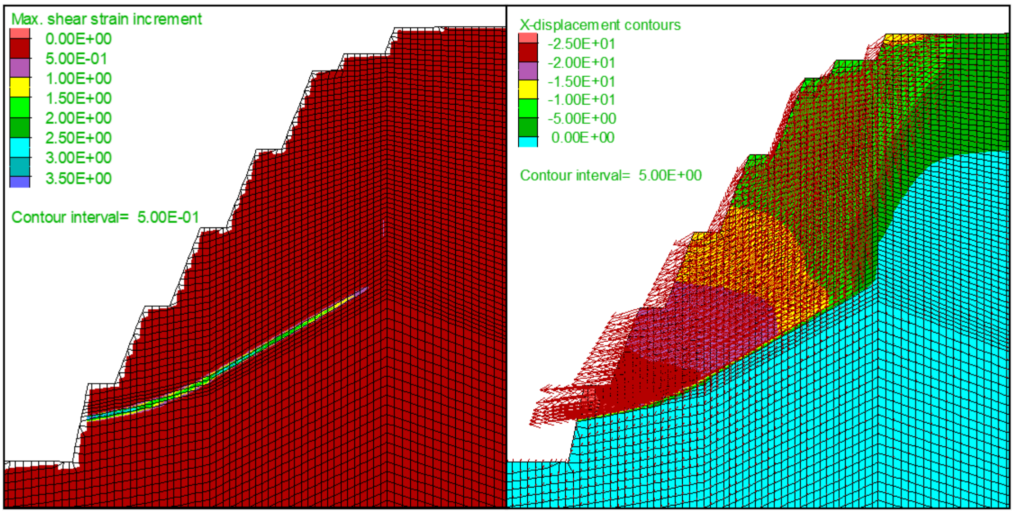

Figure 10 FLAC analysis of the northeast portion of the headscarp approximately corresponding to section A-A' (Figure 9)

The simplified strain-weakening model of the contact material illustrated the localisation and accumulation of shear strains along the base of the Qal, leading to strength loss and ultimately collapse. However, the effect of mining-induced relaxation and deformation of the bedrock underlying the Qal and Tal/Trt during the initial phases of mining prior to 2013 was not evaluated in detail at the time. Further analysis evaluating mining-induced stress relaxation leading up to the 2013 event could provide additional insight to the failure mechanism and time-dependent history of instability.

5 Discussion

The 2013 slope failure was interpreted at the time to be the result of 3 key factors:

- Mining near the toe of the slope induced relaxation and deformations of the intrusive bedrock, possibly exacerbated by excess pore pressures behind a fault in the intrusive.
- Shear strain localisation in the Tal/Trt at the base of the Qal.
- A reduction in shear strength of the Tal/Trt due to shear straining (strain-weakening).

The progressive nature of the failure was evidenced by prism monitoring, which recorded increasing deformation in the slope, and by the development of cracking at the slope crest and face months before the collapse. Notably, the failure did not occur until mining had advanced approximately 5 benches into the intrusive below the base of the Qal, fully daylighting the presumed slip surface months prior to the event. Prior to signs of instability, the Qal in the south highwall was mined at inter-ramp slope angles greater than 55° and performed very well. Martin & Stacey (2018) contains additional information on the history of slope performance in the cemented alluvial slopes.

Additionally, several slopes in the Qal in East Archimedes continue to stand at heights greater than the failed portion of the slope. The 2D and 3D limit equilibrium slope stability analyses indicated unstable conditions when the residual shear strengths from laboratory testing and slope stability back-analyses were applied.

Although the strain-weakening model provided a useful conceptual model for the 2013 failure, predicting future slope performance proved challenging for several reasons:

- The character, structure, and distribution of alteration in the bedrock is complex, making accurate modelling difficult, and deformation of the bedrock appears to be a contributing factor to instability in the Qal.
- The localisation of cumulative shear strains along the contact during mining is difficult to replicate accurately.
- Shear strength reduction of the contact material was likely the result of several factors, some of which may be time-dependent, such as those observed in stiff clays (Skempton 1964).

Uncertainty remains regarding the precise mechanisms of progressive failure in both the 2013 and 2022 events. The stability analyses conducted on the 2013 event are based on a model in which shear straining in the Tal/Trt is the result of gravity loading. However, stiffness incompatibility (i.e. differential elastic modulus) between the Qal and underlying bedrock may also have contributed to strain localisation and weakening in the Tal/Trt, similar to that described by Martin & Stacey (2013, 2018) and Zobolotnii et al. (2022).

Collins & Sitar (2001) suggest that in steep slopes in moderately cemented sands, the controlling mechanism is tensile failure rather than shear failure, and traditional limit equilibrium stability analyses generally do not accurately capture this failure mode. The backplane angles predicted by both limit equilibrium and FLAC analyses do not align well with the near-vertical headscarp observed in the field, suggesting that an alternative to the shear sliding failure mode may be plausible.

The timing of the 2022 failure, occurring shortly after additional mining in 2021 in the East Archimedes pit which had been inactive for several years, suggests a connection between bedrock deformation and the subsequent failure. However, it is possible that other factors, such as surface water infiltration or time-dependent strain-weakening, played a role, and the timing of the 2022 collapse and mining was coincidental.

6 Conclusion

The 2013 and 2022 slope failures in the East Archimedes pit highlight the challenges of evaluating slope stability in complex geologic environments, particularly involving heterogeneous materials, strain-weakening properties, and potentially time-dependent behaviour. Stability of the East Archimedes alluvium slopes appears to be sensitive to mining-induced stress changes in the bedrock, yet the precise mechanism of failure and controlling factors contributing to instability remain uncertain. Additional detailed modelling in the future may provide added insights to the behaviour of the slopes.

Acknowledgement

The authors would like to thank i-80 Gold Corp. for the use of the data and case history summarised in this paper.

References

ASTM International 2025, *Classification of Soils for Engineering Purposes (Unified Soil Classification System (D2487-17)*, West Conshohoken.

Collins, B & Sitar, N 2011, 'Stability of steep slopes in cemented sands', *Journal of Geotechnical and Geoenvironmental Engineering*, vol. 137, no. 1, http://dx.doi.org/10.1061/(ASCE)GT.1943-5606.0000396

Martin, CD & Stacey, PF 2013, 'Pit slopes in weathered and weak rocks', in PM Dight (ed.), *Slope Stability 2013: Proceedings of the 2013 International Symposium on Slope Stability in Open Pit Mining and Civil Engineering*, Australian Centre for Geomechanics, Perth, pp. 3–28, https://doi.org/10.36487/ACG_rep/1308_0.1_Martin

Martin, CD & Stacey, PF 2018, 'Chapter 6: cemented sediments', *Guidelines for Open Pit Slope Design in Weak Rocks*, CRC Press, Boca Raton.

Skempton, A W 1964, 'Long-term stability of clay slopes', *Géotechnique*, vol. 14, no. 2, pp. 77–101.

Zobolotnii, E, Morgenstern, NR & Wilson GW 2022, 'Asynchronous mobilization of shear resistance in slope failures', *ISSMGE International Journal of Geoengineering Case Histories*, pp. 54–72, https://doi.org/10.4417/IJGCH-06-03-03